


Cite this: *Mater. Adv.*, 2022,  
3, 6028

# Engineering of a self-supported carbon electrode with 2D ultrathin heterostructures of NiCo LDH/NiCoS *via* a MOF-template for sensitive detection of glucose and H<sub>2</sub>O<sub>2</sub>†

Lili Wang,<sup>\*a</sup> Jiahui Li,<sup>a</sup> Yibing Zhao,<sup>b</sup> Haojia He,<sup>b</sup> Linlin Zheng,<sup>a</sup> Zejia Huang,<sup>b</sup> Xu Zhao,<sup>b</sup> Junqing Xu,<sup>c</sup> Bing Wang<sup>\*a</sup> and Zhen Yin <sup>\*d</sup>

Reasonable design and development of bifunctional electrodes for glucose and hydrogen peroxide (H<sub>2</sub>O<sub>2</sub>) detection are of great significance since glucose and H<sub>2</sub>O<sub>2</sub> levels are important indicators for evaluating environmental and dietary health. In this work, we develop a simple and efficient strategy to fabricate self-supported and low-cost carbon electrodes consisting of two-dimensional (2D) ultrathin heterostructures of NiCo layered double hydroxide (LDH)/NiCoS array nanostructures and a carbon cloth (CC) substrate *via* a hard template method, exhibiting superior detection performances for glucose and H<sub>2</sub>O<sub>2</sub>. A 2D Co MOF is employed as a sacrificial template and a Co source for the growth of NiCo LDH, which can also ensure the anchoring and stability of the nanosheet. Owing to the interface and the 2D ultrathin structure of NiCo LDH/NiCoS, the obtained self-supported carbon electrode shows excellent sensitivities for glucose oxidation (2167 and 1417  $\mu\text{A mM}^{-1} \text{cm}^{-2}$ ) and H<sub>2</sub>O<sub>2</sub> reduction (285  $\mu\text{A mM}^{-1} \text{cm}^{-2}$ ) with significant anti-interference and a low detection limit. The stronger electronic interaction at the hybrid interface between NiCo LDH and NiCoS facilitates the adsorption of reactants and the desorption of products, and promotes the rapid response of the electrode to glucose and H<sub>2</sub>O<sub>2</sub>. Our present work demonstrates an efficient way *via* a combination of bimetallic sulfides and LDH for improving the electrochemical sensing of electrodes, revealing the significant potential of low-cost bifunctional electrodes with 2D ultrathin nanostructures and a carbon substrate for detection.

Received 23rd April 2022,  
Accepted 14th June 2022

DOI: 10.1039/d2ma00454b

rsc.li/materials-advances

## 1. Introduction

Diabetes, as a chronic disease that causes systemic and metabolic disorders, threatens the lives and health of many people around the world. Excessive sugar intake can cause various chronic diseases, such as obesity and cardiovascular and cerebrovascular diseases.<sup>1,2</sup> In the process of clinical diagnosis, accurate and rapid determination of the blood glucose level is very important for all stages of treatment and disease management. Therefore, glucose detection is an important indicator of food manufacturing and medical health.<sup>3</sup> Meanwhile, H<sub>2</sub>O<sub>2</sub>

produced by the metabolism of the human body can be present in different biological tissue compartments by freely penetrating the cell membrane, which is toxic to the human body.<sup>4</sup> It is considered to be one of the main risk factors for life-threatening diseases related to oxidative stress. In particular, H<sub>2</sub>O<sub>2</sub> is closely related to the development of neurological diseases such as Alzheimer's disease and Parkinson's disease. Hence, it is important to develop efficient techniques for the dual detection of glucose and H<sub>2</sub>O<sub>2</sub>, which is critical for the assessment of biological and environmental health.

In the past decades, the electrochemical methods have attracted tremendous research interest for the quantitative detection of glucose and H<sub>2</sub>O<sub>2</sub> due to many fascinating features, including excellent sensitivity, high accuracy and easy operation. For example, enzyme-based biosensors have been widely studied and used since the first device was developed by Clark and Lyons in 1962, which employed glucose oxidase to oxidize glucose in the presence of oxygen. However, traditional enzyme-based electrochemical sensors are generally limited due to various environmental factors, such as temperature, solution pH and toxic chemicals.<sup>5</sup> In addition, the loss of enzyme biological activity

<sup>a</sup> State Key Laboratory of Separation Membranes and Membrane Processes, School of Chemistry, Tiangong University, Tianjin 300387, China.

E-mail: wanglili@tiangong.edu.cn, bingwang@tiangong.edu.cn

<sup>b</sup> School of Chemical Engineering and Technology, Tiangong University, Tianjin 300387, China<sup>c</sup> China Tianchen Engineering Corporation, Tianjin 300400, China<sup>d</sup> College of Chemical Engineering and Materials Science, Tianjin University of Science and Technology, Tianjin 300457, China. E-mail: yinzheng@tust.edu.cn† Electronic supplementary information (ESI) available: SEM, TEM, XRD, XPS, CV, and *i*-*t*. See DOI: <https://doi.org/10.1039/d2ma00454b>

caused by denaturation and inherent instability will also affect the test results. These factors can be avoided by replacing biological enzymes with active materials on electrodes for electrocatalytic sensing. This is mainly based on the redox reaction and fast electron transfer to achieve the purpose of detection, and thus possesses a short response time and good stability.<sup>6,7</sup>

Currently, numerous studies are devoted to exploring efficient electrocatalysts based on nanomaterials, mainly including noble metal and non-noble metal-based ones. Considering cost-effectiveness and raw material reserves, transition metal catalysts as typical non-noble metals have gained more extensive research than noble metal-based catalysts.<sup>8,9</sup> Transition metal-based nanomaterials exhibit excellent catalytic activity in the application of enzyme-free sensors due to their abundant active sites, high electrical conductivity and ease of functionalization. The rational design of nanomaterials is beneficial to increase the electrochemical active surface area, accelerate the electron transfer rate and improve the stability. In recent years, multi-component materials exhibited impressive activity in the field of glucose and H<sub>2</sub>O<sub>2</sub> sensing owing to the stronger interfacial synergy and electronic coupling effects than a single component. For example, three-dimensional (3D) bimetallic compounds (Ni-Co PBA HNCs) have been reported to exhibit superior glucose catalytic oxidation activity with high sensitivity (149  $\mu\text{A mM}^{-1} \text{cm}^{-2}$ ) compared to single Ni PBA HNCs and Co PBA HNCAs.<sup>10</sup> Co<sub>3</sub>O<sub>4</sub>@NiCo<sub>2</sub>O<sub>4</sub> nanosheets with a porous hybrid structure were applied for glucose and H<sub>2</sub>O<sub>2</sub> sensing, achieving high sensitivities (1463.13 and 303.42  $\mu\text{A mM}^{-1} \text{cm}^{-2}$ ).<sup>11</sup> On the other hand, 2D nanomaterials have been reported for extensive applications due to their absolute openness and effective interaction with external stimuli.<sup>12</sup> Typical 2D materials such as LDHs have also attracted considerable research interest in electrochemical sensors owing to their reliable physicochemical stability and higher surface area. It has been reported that the hybrids (NiMn-LDH/GO) of NiMn-LDH assembled on graphene oxide (GO) can effectively detect H<sub>2</sub>O<sub>2</sub> and glucose with sensitivities of 96.82 and 839.2  $\mu\text{A mM}^{-1} \text{cm}^{-2}$ , respectively.<sup>13</sup> The interconnected 3D structure was obtained by hydrothermally growing NiCo LDH on CC with a sensitivity of 5.12  $\mu\text{A mM}^{-1} \text{cm}^{-2}$  for glucose detection.<sup>14</sup> However, the research on the bifunctional detection of glucose and H<sub>2</sub>O<sub>2</sub> based on 2D multi-transition metal LDHs is still in the initial stage, and the conductivity and activity of such materials need to be improved.

Transition metal sulfides (TMS) are considered as a promising material for sensing electrodes owing to their excellent electrical conductivity and redox activity.<sup>15,16</sup> In particular in the interior of nanomaterials, it is easy to construct a multi-component heterogeneous interface in the process of ion exchange with S<sup>2-</sup>, which promotes the reduction of the surface energy of the material.<sup>17</sup> Since the electrochemical reaction of TMS always occurs on the surface or interface of an electrode material, and the ultrathin structure of the TMS material has abundant specific surface areas and defects, it can provide more active sites for electrochemical sensing. For example, the NiS nanoparticles prepared by electrodeposition showed excellent redox properties for glucose and H<sub>2</sub>O<sub>2</sub>, reaching sensitivities of

25.71 and 0.498  $\mu\text{A } \mu\text{M}^{-1}$  with detection ranges of 1–1000 and 1–5000  $\mu\text{M}$ .<sup>18</sup> In addition, it has been reported that bimetallic sulfides have more attractive electrochemical properties based on the synergistic effect between different metals than single sulfides. A Zn-Co-S ball-in-ball hollow sphere (BHS) was obtained *via* ion exchange and a sulfidation method for highly selective glucose detection with a sensitivity of up to 2734.4  $\mu\text{A mM}^{-1} \text{cm}^{-2}$  and a wide detection range of 5–100  $\mu\text{M}$ .<sup>19</sup> Ni<sub>2.5</sub>Mo<sub>6</sub>S<sub>6.7</sub> was grown on poly(3,4-ethylenedioxythiophene)-reduced graphene oxide (PEDOT-rGO) hybrid membranes *via* electrodeposition to obtain Ni<sub>2.5</sub>Mo<sub>6</sub>S<sub>6.7</sub>/PEDOT-rGO with high sensitivities toward glucose (666.67 and 266.10  $\mu\text{A mM}^{-1} \text{cm}^{-2}$ ) and H<sub>2</sub>O<sub>2</sub> (1273.52  $\mu\text{A mM}^{-1} \text{cm}^{-2}$ ).<sup>20</sup> However, the multiple electron transfer reactions in the detection process make TMS less reversible, resulting in unsatisfactory stability. In addition, the preparation of TMS faces problems such as desulfurization or accumulation of sulfides. Therefore, it is still necessary to explore more convenient methods to construct exquisite morphology and structure for ensuring the orderly and efficient electrochemical reaction.

Although TMS and LDH nanomaterials have been reported for their excellent electrochemical properties, most of them are powders without support, which face several critical issues, such as time-consuming preparation of electrodes, addition of binders and aggregation of particles. Recently, the self-supported electrodes obtained through direct growth of active materials on various conductive substrates have been demonstrated as an efficient electrode for the detection. Among them, the self-supported electrode based on the CC has been regarded as one of most promising electrodes due to good conductivity, mechanical stability and a wide voltage range.<sup>21</sup> Moreover, the excellent biocompatibility of CC promotes higher catalytic efficiency, which is attributed to the expansion of the surface area of carbon fiber with a 3D structure and high loading amount for active substances.<sup>22</sup> If the 2D ultrathin hybrid nanostructures based on the TMS can be directly anchored on the CC, the remarkable electrochemical detection performance of self-supported carbon electrodes may be achieved due to their unique advantages and synergy effect of the active TMS and carbon substrates. To date, 2D ultrathin self-supported nanostructures based on rich interfaces dedicated to the bifunctional detection of glucose and H<sub>2</sub>O<sub>2</sub> have rarely been reported.

In this work, a self-supported carbon electrode is constructed with the 2D ultrathin nanostructure of hybrid NiCo LDH/NiCoS arrays and CC as the substrate, which can be used for bifunctional detection of glucose and H<sub>2</sub>O<sub>2</sub>. Firstly, a 2D Co MOF was grown at room temperature as a sacrificial template, and then Co MOF was ion exchanged with Ni<sup>2+</sup> to obtain NiCo LDH. Finally, a surface sulfidation method was used to construct the 2D hybrid NiCo LDH/NiCoS nanostructures. The obtained NiCo LDH/NiCoS/CC electrode exhibits a superior electrochemical sensing performance for the detection of glucose and H<sub>2</sub>O<sub>2</sub> due to ultrathin 2D nanosheets and abundant interfaces between LDH and NiCoS. As a glucose sensor, it has wide detection ranges (1  $\mu\text{M}$ –3 mM and 4–9 mM) with excellent sensitivities of 2167 and 1417  $\mu\text{A mM}^{-1} \text{cm}^{-2}$ ,



an extremely short response time (within 2 s) and a low detection limit of 208 nM. When the electrode is applied to  $\text{H}_2\text{O}_2$  sensing, it also exhibits a reasonable detection range (10  $\mu\text{M}$  to 12 mM) and higher sensitivity (285  $\mu\text{A mM}^{-1} \text{cm}^{-2}$ ) with a lower detection limit (1.66  $\mu\text{M}$ ). Moreover, the NiCo LDH/NiCoS/CC electrode has significant anti-interference, reproducibility and stability. Our present work demonstrates that the self-supported carbon electrode with NiCo LDH/NiCoS and CC would be a promising and low-cost self-supported electrode in the field of detection.

## 2. Experimental section

### 2.1 The experimental materials

All reagents were analytical grade reagents and no further purification was required. 2-Methylimidazole ( $\text{C}_4\text{H}_6\text{N}_2$ ), cobalt nitrate hexahydrate ( $\text{Co}(\text{NO}_3)_2 \cdot 6\text{H}_2\text{O}$ ), nickel nitrate hexahydrate ( $\text{Ni}(\text{NO}_3)_2 \cdot 6\text{H}_2\text{O}$ ), thioacetamide (TAA), ethanol absolute, sodium hydroxide (NaOH), glucose, hydrogen peroxide (30%), sucrose (Suc), lactose (Lac), fructose (Fru), ascorbic acid (AA), uric acid (UA), sodium chloride (NaCl), potassium chloride (KCl), dopamine (DA), and L-cysteine (Cys) were purchased from Shanghai Macklin Biochemical Co., Ltd, and carbon cloth (CC) was purchased from Suzhou Siner Technology Co., Ltd.

### 2.2 Preparation of NiCo LDH/NiCoS

In our reported work,<sup>23</sup> NiCo LDH/NiCoS/CC has been successfully prepared. Specifically, Co MOF was first grown on carbon cloth for 4 h at room temperature, then etched in  $\text{Ni}^{2+}$  ethanol solution for 2 h, and finally surface sulfidation was carried out using a hydrothermal method for 4 h.

### 2.3 Material characterization

The morphology and structure of the sample were observed using a cold field emission scanning electron microscope (SEM, Hitachi Regulus 8100, Japan), transmission electron microscope (TEM, Hitachi H7650, Japan) and field emission high resolution transmission electron microscope (HR-TEM, JEM-F200, Japan). The crystal structure of the samples was characterized *via* an X-ray diffractometer (D8 ADVANCE, BRUKER) with Cu-K $\alpha$  radiation. The element composition and chemical valence were determined by X-ray photoelectron spectroscopy (XPS, NEXSA, Thermo Fisher).

### 2.4 Electrochemical measurement

In this work, all electrochemical-related tests were carried out on an electrochemical workstation (CHI 760E). Under the three-electrode system, the prepared NiCo LDH/NiCoS/CC ( $1 \times 1 \text{ cm}^2$ ) can be directly used as the working electrode, a platinum electrode ( $1 \times 1 \text{ cm}^2$ ) was employed as the counter electrode and Hg/HgO was used as the reference electrode. In addition, the tests related to glucose and  $\text{H}_2\text{O}_2$  sensing were performed under alkaline condition (0.5 M NaOH). Before the electrochemical test, cyclic voltammetry (CV) was used to activate the electrode material to ensure the wettability of the material,

which is more conducive to good contact between the material and the electrolyte. In order to study the electrochemical activity and stability of the NiCo LDH/NiCoS/CC electrode towards glucose and  $\text{H}_2\text{O}_2$ , CV curves were obtained under voltage windows of  $-0.1$  to  $0.7$  and  $-0.7$  to  $-0.1$  V at different scan rates, respectively. The sensitivity and anti-interference of the electrodes were evaluated using amperometric *i-t* curves under magnetic stirring.

## 3. Results and discussion

### 3.1 Characterization of the structure and morphology

As shown in Fig. 1, the synthesis of the ultrathin NiCo LDH/NiCoS/CC electrode consists of the following three steps. Firstly, 2D nanosheet precursors of Co MOF were directly grown on CC by solution deposition at room temperature. Then the NiCo LDH nanosheets were formed on the original smooth surface of Co MOF *via* ion exchange with  $\text{Ni}(\text{NO}_3)_2 \cdot 6\text{H}_2\text{O}$ . The growth mechanism was based on the high hydrolysis rate of  $\text{Ni}(\text{NO}_3)_2 \cdot 6\text{H}_2\text{O}$  in ethanol solution.<sup>24</sup> During the hydrolysis of metal ions, a large number of  $\text{H}^+$  protons was generated and began to corrode the surface of Co MOF, and the thickness of Co MOF gradually reduced.<sup>25</sup> At the same time, ethanol acted as a solvent to help the diffusion of  $\text{Co}^{2+}$  in the Co MOF and prevented the destruction of the MOF structure, and  $\text{Co}^{2+}$  may be partially oxidized.<sup>26–28</sup> Then the  $\text{Ni}^{2+}$  and  $\text{Co}^{2+}/\text{Co}^{3+}$  in the solution can react with  $\text{OH}^-$  to form NiCo hydroxide seed crystals attached to the surface of the Co MOF and continue to grow, thus producing uniform and tiny NiCo LDH nanosheets and maintaining the original structure of the precursor. Finally, the NiCo LDH/NiCoS was prepared by the solvothermal method. In this process, the loss of some Co and Ni atoms caused part of the NiCo LDH nanosheets to disappear.<sup>29</sup> Therefore, the NiCo LDH/NiCoS/CC electrode had a unique 2D ultrathin nanostructure, which can greatly reduce the internal resistance and promote the rapid occurrence of catalytic reactions.

The SEM and TEM images of the sacrificial template (2D Co MOF) and the ion exchange product (NiCo LDH) are shown in

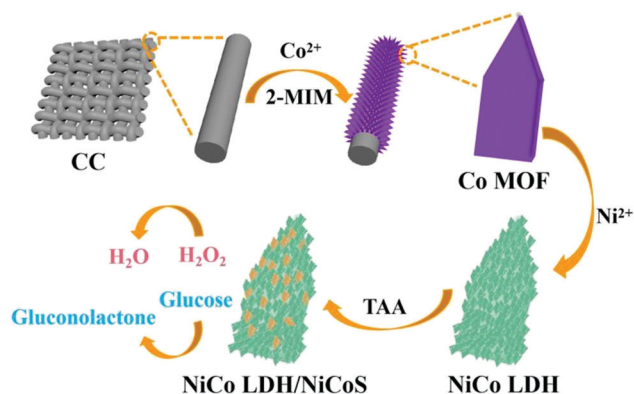


Fig. 1 Schematic illustration of the preparation of NiCo LDH/NiCoS/CC electrodes.



Fig. S1 (ESI†). The surface of the pristine Co MOF is smooth and flat with clear edges. NiCo LDH is slightly curled, and tiny nanosheets are grown on the surface. XRD pattern indicates the phase transformation from the Co MOF phase to the NiCo LDH/NiCoS heterostructure (Fig. S2, ESI†). In Fig. S3 (ESI†), the presence of Ni, Co, O, C, and S elements proves that NiCo LDH/NiCoS/CC has been successfully prepared. The morphology and structure of NiCo LDH/NiCoS hybrid nanoarrays are studied by SEM, TEM and HRTEM analysis, as shown in Fig. S4 (ESI†). It can be seen that the ultrathin NiCo LDH/NiCoS nanoarrays are uniformly grown on the CC, and there are many small wrinkles on the surface of the nanosheets (Fig. S4a and b, ESI†). The TEM image (Fig. S4c, ESI†) shows that NiCo LDH/NiCoS forms a layered structure while retaining the 2D Co MOF framework. The ingenious structure ensures that the NiCo LDH/NiCoS on the CC are vertically arranged and stable, avoiding detachment of the nanostructure from the electrode surface and aggregation of nanosheets during the electrochemical reaction process. Furthermore, Fig. S4d (ESI†) confirms the formation of an interface between NiCo LDH and NiCoS.

### 3.2 Electrochemical behavior towards glucose sensing

Considering the important influence of electrolyte concentration on electrocatalytic behavior, the optimum NaOH concentration is selected using a CV test, and the oxidation peak current densities are marked in the form of a histogram (Fig. S5, ESI†).<sup>30</sup> The peak current density progressively increases and then decreases when the concentration of NaOH raises from 0.5 to 1.5 M. The current response is the highest when the OH<sup>−</sup> concentration is 0.5 M, indicating that an appropriate concentration of OH<sup>−</sup> is beneficial to the conversion of Co<sup>2+</sup>/Co<sup>3+</sup> and Ni<sup>2+</sup>/Ni<sup>3+</sup>, and improves the kinetics of

glucose oxidation. However, excessive OH<sup>−</sup> causes the isomerization of glucose and the accumulation of negative charges on the surface of the electrode, affecting the diffusion and adsorption of glucose.<sup>31</sup> The redox reaction mechanism of the electrode in alkaline solution is as follows:<sup>14,32,33</sup>

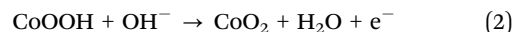
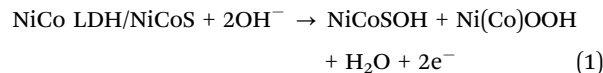
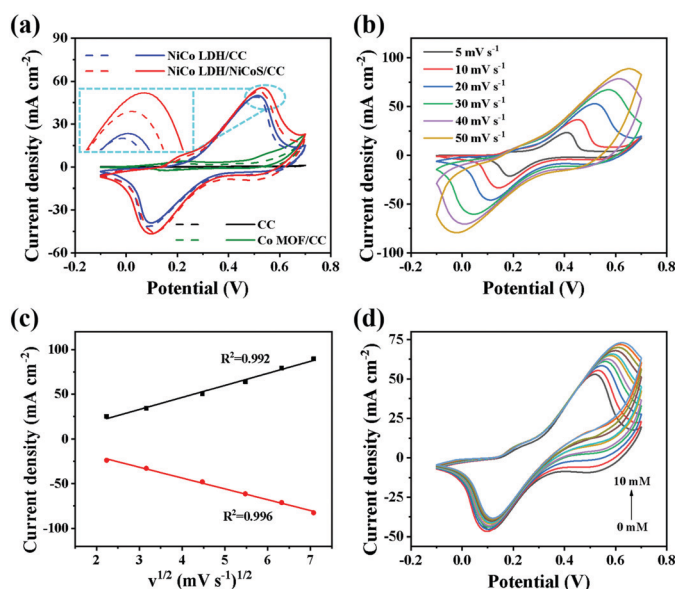


Fig. 2a shows the CV curves of NiCo LDH/NiCoS/CC and control electrodes (CC, Co MOF/CC and NiCo LDH/CC) in the presence (solid line) and absence (dashed line) of 1 mM glucose in 0.5 M NaOH at 20 mV s<sup>−1</sup>. Obviously, the current response of the NiCo LDH/NiCoS/CC electrode is the largest, indicating that it has an outstanding catalytic oxidation effect on glucose. Furthermore, oxidation peaks around 0.2 and 0.5 V for NiCo LDH/NiCoS/CC can be clearly seen, which are attributed to Co<sup>2+</sup>/Co<sup>3+</sup> and Ni<sup>2+</sup>/Ni<sup>3+</sup>, Co<sup>3+</sup>/Co<sup>4+</sup>.<sup>34–37</sup> In addition, to demonstrate that the 2D ultrathin heterostructure plays an important role in improving the detection capability of the electrode, we also prepared two control electrodes (NiCoS/CC and Co MOF/NiCoS/CC), as shown in Fig. S6 (ESI†). Fig. S7 (ESI†) shows the CV curves of the control electrodes for glucose detection. It is difficult for NiCoS to grow directly on CC uniformly, resulting in an insignificant current response to glucose, which indicates that Co MOF can guarantee the stability of the electrode. Co MOF/NiCoS/CC is obtained by growing NiCoS on Co MOF without ion exchange. Although there is a current response to glucose oxidation, it is much lower than that of NiCo LDH/NiCoS/CC, confirming that the formation of NiCo LDH is more favorable for electron transfer, increasing the specific surface

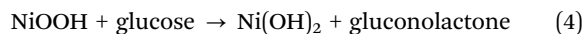


**Fig. 2** (a) CV curves of the CC, Co MOF/CC, NiCo LDH/CC and NiCo LDH/NiCoS/CC electrodes in the presence (solid line) and absence (dashed line) of 1 mM glucose in 0.5 M NaOH at a scan rate of 20 mV s<sup>−1</sup>. (b) CV curves of the NiCo LDH/NiCoS/CC electrode with 1 mM glucose in 0.5 M NaOH at a scan rate of 5–50 mV s<sup>−1</sup>. (c) The fitting of the corresponding peak current density value vs.  $v^{1/2}$ . (d) CV curves of the NiCo LDH/NiCoS/CC electrode in 0.5 M NaOH containing various concentrations of glucose at a scan rate of 20 mV s<sup>−1</sup>.



area and anchoring NiCoS. The above results indicate that the ultrathin heterostructure with an abundant interface of NiCo LDH/NiCoS further enriches more active sites and improves the kinetics of the electrocatalytic reaction, thereby promoting the oxidation of glucose.

Fig. 2b indicates that the anode peak moves toward the positive potential with the enhancement of scan rates, while the cathode peak moves toward the negative potential, possibly due to the kinetic limitation in the diffusion layer which was created at a high current density.<sup>38,39</sup> Moreover, as shown in Fig. 2c, the anodic and cathodic current densities increase linearly with  $v^{1/2}$ , indicating that the glucose oxidation process on the electrode surface is affected by the glucose concentration in the electrolyte and the entry of glucose into the electrode and electrolyte interface,<sup>31,40</sup> suggesting that the glucose oxidation over the as-prepared NiCo LDH/NiCoS/CC electrode may be controlled by diffusion. We also plotted the relationship between  $\log v$  and  $\log I_{pa}$ , as shown in Fig. S8 (ESI<sup>†</sup>), confirming good linearity. The regression equation is:  $\log I_{pa} \text{ (mA cm}^{-2}\text{)} = 0.56 \log v \text{ (mV s}^{-1}\text{)} + 0.98$ ,  $R^2 = 0.995$ . According to the electrochemical process theory, when the slope of the linear relationship is 0.5, it is a diffusion-controlled electrode reaction. When the slope is 1, there is a surface-controlled reaction process. The slope of this equation (0.56) is much closer to the theoretically expected value of 0.5, indicating a dominant diffusion-controlled process mixed with a possible surface-controlled process over the NiCo LDH/NiCoS/CC electrode.<sup>39,41–43</sup> In Fig. 2d, the anode peak current density is proportional to the glucose concentration, and the value of peak potential moves to the positive direction, demonstrating that the NiCo LDH/NiCoS/CC electrode exhibits excellent catalytic activity in a wide concentration range. However, the current change is not obvious when the glucose concentration reaches 10 mM. The possible reason is that a small amount of glucose and oxidized intermediates are adsorbed and accumulated on the surface of the electrode with the increasing glucose concentration, which hinders the contact and diffusion of glucose with the active substance. The possible reaction process with glucose is expressed by the following chemical equation:<sup>14,44,45</sup>



The applied potential is an important factor for measuring the performance of electrochemical sensing. The potential near the oxidation peak (0.4 to 0.55 V) is selected for exploration. Fig. 3a and Fig. S9 (ESI<sup>†</sup>) record the corresponding amperometric response and fitting relationship when 0.1 mM glucose is continuously injected into 0.5 M NaOH. The current response rises in steps with the glucose concentration and +0.5 V is an appropriate applied voltage. This is because the background current generated by the electrode is small at +0.5 V, and the

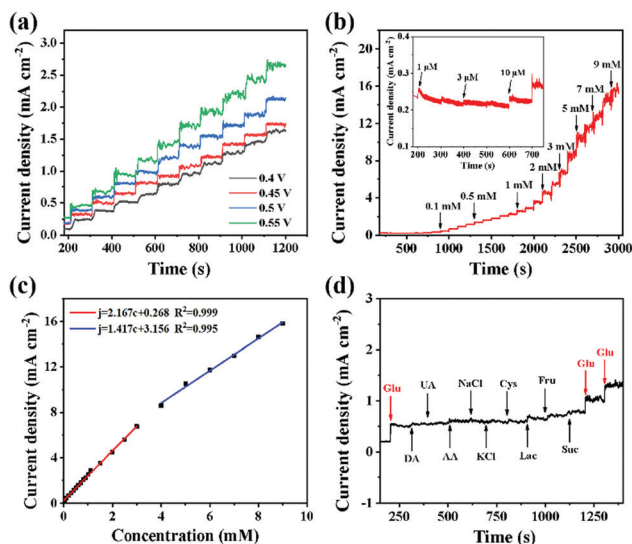


Fig. 3 Responses of glucose oxidation with the obtained NiCo LDH/NiCoS/CC electrodes: (a) at different applied potentials, (b) with different concentrations of glucose in 0.5 M NaOH at +0.5 V, (c) relationship of the current densities vs. glucose concentration and (d) interference test with the injection of interfering species (0.1 mM) in 0.5 M NaOH at +0.5 V.

current response platform is stable, indicating that the detection at this voltage has good stability and higher accuracy. Although the current response is higher when the applied voltage is +0.55 V, there is an inevitable shortcoming of large background current and the measurement baseline begins to be unstable when the time and concentration reach a certain range. For subsequent electrochemical measurements, an appropriate potential can prevent excessive reaction products from blocking the active sites, which is more conducive to the oxidation of glucose.<sup>31</sup>

According to the optimized conditions, the amperometric response of adding different concentrations of glucose every 100 s is recorded within 3000 s under constant stirring. As shown in Fig. 3b, the current increases steadily in a stepwise manner with the addition of glucose. From the partial magnification, the current begins to respond significantly when 1  $\mu\text{M}$  glucose is injected. In fact, the current curve begins to fluctuate when the concentration of glucose reaches 9 mM and the stable current platform basically disappears, indicating that the oxidation of glucose is close to saturation.<sup>46</sup> In Fig. 3c, the sensitivities in two concentration ranges (1  $\mu\text{M}$ –3 mM and 4–9 mM) are obtained by the slope, which are 2167 and 1417  $\mu\text{A mM}^{-1} \text{ cm}^{-2}$ , respectively. According to the calculation equation of LOD ( $\text{LOD} = 3S_b/K_i$ ,  $S/N = 3$ ), the minimum detection limit is calculated to be 208 nM, where  $S_b$  and  $K_i$  are the standard deviation of the blank solution and the slope.<sup>47</sup> Moreover, the current quickly reaches a steady state within 2 s after each injection of glucose, as shown in Fig. S10 (ESI<sup>†</sup>). The detection time can be effectively shortened due to the low background current of the CC substrate and the 2D ultrathin structure. Selectivity is one of the reference indicators of electrode sensing performance. The effects of common interferences such as Suc, Fru, Lac, Cys, KCl, NaCl, AA, UA and DA on glucose sensing are investigated.<sup>48,49</sup> In Fig. 3d, the NiCo LDH/NiCoS/CC

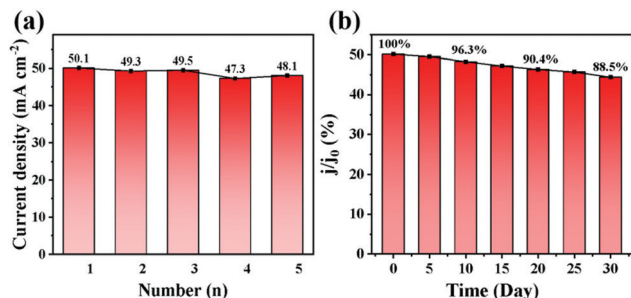


Fig. 4 (a) Reproducibility and (b) stability test of the NiCo LDH/NiCoS/CC electrodes in 0.5 M NaOH containing 1 mM glucose.

electrode has not shown a significant current response with the injection of interferences (0.1 mM), while the current response increases rapidly after 0.1 mM glucose injection, indicating a good anti-interference performance.<sup>50,51</sup>

In addition, as shown in Fig. 4a, five electrodes are prepared to evaluate the reproducibility of the electrodes. Each electrode is prepared *via* the same procedure under the same conditions. The oxidation peak current responses of the electrodes are collected *via* CV testing. The relative standard deviation (RSD) is 2.3%, confirming excellent reproducibility. The stability is measured based on the current response of the electrode to glucose within 30 days. Fig. 4b displays the current response of a naturally placed electrode to 1 mM glucose (tested every 5 days) and the value of current response drops by only 11.5% in 30 days, revealing that the electrode has superior stability and potential in the field of glucose sensing.

### 3.3 Electrochemical behavior towards H<sub>2</sub>O<sub>2</sub> sensing

The sensing performance of the NiCo LDH/NiCoS/CC electrode for H<sub>2</sub>O<sub>2</sub> is also studied. In Fig. S11 (ESI<sup>†</sup>), according to the sensitivity of the electrode toward 5 mM H<sub>2</sub>O<sub>2</sub> reduction in different NaOH concentrations at 50 mV s<sup>-1</sup>, 0.5 M NaOH was selected as the optimum electrolyte for subsequent tests. Compared with other control electrodes, the current density of the reduction peak with the obtained NiCo LDH/NiCoS/CC electrode displays dramatically increases when 1 mM H<sub>2</sub>O<sub>2</sub> is added to 0.5 M NaOH at a scan rate of 50 mV s<sup>-1</sup>, indicating that the NiCo LDH/NiCoS/CC electrode exhibited superior sensitivity toward H<sub>2</sub>O<sub>2</sub> and an excellent electrocatalytic performance (Fig. 5a). Furthermore, Fig. S12 (ESI<sup>†</sup>) shows that NiCoS/CC and Co MOF/NiCoS/CC electrodes are less sensitive to H<sub>2</sub>O<sub>2</sub> reduction compared with that of NiCo LDH/NiCoS/CC electrodes, revealing the superiority of the hybrid interface. Fig. S13 (ESI<sup>†</sup>) shows the CV curves of the NiCo LDH/NiCoS/CC electrode toward 3 mM H<sub>2</sub>O<sub>2</sub> at different scan rates and the fitting linear relationship between  $\nu^{1/2}$  and current densities of the reduction peak, indicating the NiCo LDH/NiCoS/CC electrode is diffusion-controlled for the H<sub>2</sub>O<sub>2</sub> reduction process. According to other previous reports, the reduction mechanism of H<sub>2</sub>O<sub>2</sub> may be described as follows (M = Ni, Co):<sup>11,52,53</sup>

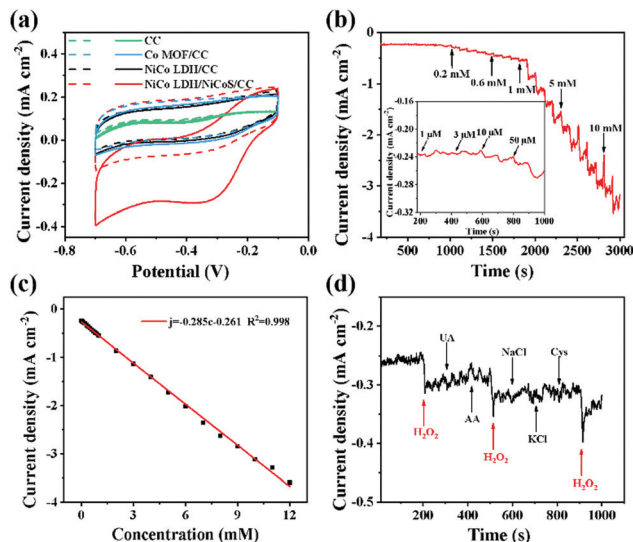
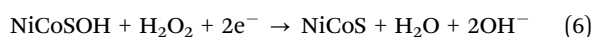
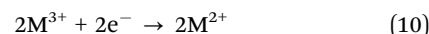
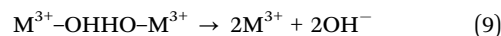
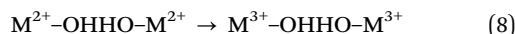
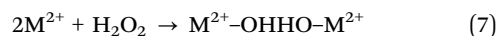


Fig. 5 (a) CV curves of the CC, Co MOF/CC, NiCo LDH/CC and NiCo LDH/NiCoS/CC electrodes in 0.5 M NaOH in the presence (solid line) and absence (dashed line) of 1 mM H<sub>2</sub>O<sub>2</sub>, (b) response of the NiCo LDH/NiCoS/CC electrode with different concentrations of H<sub>2</sub>O<sub>2</sub> in 0.5 M NaOH under -0.35 V, (c) the relationship between the current densities and H<sub>2</sub>O<sub>2</sub> concentration, and (d) interference test of the NiCo LDH/NiCoS/CC electrode with the addition of interfering species and H<sub>2</sub>O<sub>2</sub> (0.1 mM) at -0.35 V in 0.5 M NaOH.



Firstly, H<sub>2</sub>O<sub>2</sub> is adsorbed by M<sup>2+</sup> of the electrode, and electrons are transferred from M<sup>2+</sup> to the oxygen atom of H<sub>2</sub>O<sub>2</sub>, resulting in the weakening of the O-O bond. Then O-O bond elongation and electron redistribution occur, M<sup>2+</sup> is oxidized to M<sup>3+</sup> and OH<sup>-</sup> species are released. Finally, M<sup>3+</sup> is reduced to M<sup>2+</sup> by a second H<sub>2</sub>O<sub>2</sub> molecule, which eventually leads to the formation of a second OH<sup>-</sup>.

Fig. S14a (ESI<sup>†</sup>) presents the optimal working potential for the amperometric response, which is screened by continuously adding 0.1 mM H<sub>2</sub>O<sub>2</sub> at -0.25 to -0.4 V. It can be seen that the current density rises with the increases of applied potential over the as-prepared NiCo LDH/NiCoS/CC electrode, which exhibits a relatively high amperometric response and acceptable baseline fluctuations when the working voltage increases from -0.25 to -0.35 V. However, the background current is slightly high and the response is unstable at -0.4 V. In addition, as shown in Fig. S14b (ESI<sup>†</sup>), the fitting curve has the largest coefficient of determination ( $R^2$ ) of 0.999 at -0.35 V, which can be selected as the working voltage.

The amperometric response of adding different concentrations of H<sub>2</sub>O<sub>2</sub> to 0.5 M NaOH within 3000 s and the corresponding linear fitting graphs are presented in Fig. 5b and c. The current increases in a step wise manner. The maximum steady-state

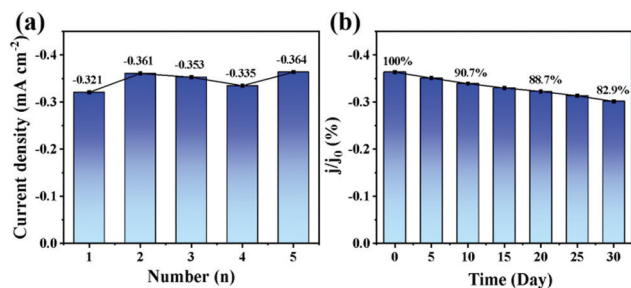


Fig. 6 (a) Reproducibility and (b) stability test of the NiCo LDH/NiCoS/CC electrodes in 0.5 M NaOH containing 1 mM  $\text{H}_2\text{O}_2$ .

current can be reached in 5 s (Fig. S15, ESI<sup>†</sup>). The current step appears obviously when the concentration of  $\text{H}_2\text{O}_2$  reaches 10  $\mu\text{M}$  (Fig. 5b). However, the current platform disappears when the concentration of  $\text{H}_2\text{O}_2$  is above 12 mM, implying that excessive concentration of  $\text{H}_2\text{O}_2$  can cause the deterioration of the electrode.<sup>54</sup> The sensitivity of the electrode is determined to be  $285 \mu\text{A mM}^{-1} \text{cm}^{-2}$  with the linear range of 10  $\mu\text{M}$ –12 mM, and the detection limit is 1.66  $\mu\text{M}$ . Similarly, the anti-interference performance of  $\text{H}_2\text{O}_2$  is evaluated by the amperometric response. Fig. 5d shows the effect of 0.1 mM anti-interference species (UA, AA, NaCl, KCl and Gys) on the current density in 0.5 M NaOH. Obviously, the introduction of interfering species does not cause a significant current response. On the contrary, the current increases rapidly after adding  $\text{H}_2\text{O}_2$ , demonstrating that the obtained NiCo LDH/NiCoS/CC electrode has an excellent anti-interference ability toward  $\text{H}_2\text{O}_2$  under negative potential.

Fig. 6a and b show the evaluation of the reproducibility and stability of the as-prepared NiCo LDH/NiCoS/CC electrode. The RSD of the current response of the five carbon electrodes to  $\text{H}_2\text{O}_2$  is 5.3% under the same preparation conditions. The current response of the electrode to  $\text{H}_2\text{O}_2$  decreases to 82.9% of the initial value after 30 days, illustrating that the obtained carbon electrode with NiCo LDH/NiCoS nanoarrays has a convincing reproducibility and stability. Based on the outstanding

application of the NiCo LDH/NiCoS/CC electrode in sensing, other previous bifunctional electrodes are compared and listed in Table 1, demonstrating that the obtained self-supported carbon electrode with NiCo LDH/NiCoS nanoarrays and CC would be an efficient and accurate enzyme-free sensor with a reasonable detection range and sensitivity.

The excellent sensing performance of NiCo LDH/NiCoS/CC can be ascribed to the advantages of hybrid 2D nanostructures and superior catalytic activity toward glucose and  $\text{H}_2\text{O}_2$ . The abundant pores of MOFs provide electron transport channels.<sup>67–69</sup> A MOF can be used as a sacrificial template, which is beneficial to well-coating and dispersion of LDH. The process of ion exchange provides conditions for forming ultrathin heterostructures. The formation of a hybrid interface with LDH can modulate the electronic structure of sulfides and obtain more high-valent metal ions,<sup>23</sup> thereby promoting the oxidation of glucose, as shown in eqn (3)–(5). And the hybrid interface will facilitate the adsorption of  $\text{H}_2\text{O}_2$ , which is beneficial to the reduction of  $\text{H}_2\text{O}_2$  (eqn (6)–(10)). The unique hybrid 2D ultrathin nanostructure can facilitate the transfer of charges and diffusion of glucose and  $\text{H}_2\text{O}_2$  molecules. Furthermore, the 2D ultrathin nanostructure can possess a high specific surface area, expose more catalytic sites, prompt the formation of intermediates and enhance the kinetics of electrocatalytic reactions. The biocompatibility and high conductivity of CC as a substrate also further enhances the stability and detection capability of the electrode. Therefore, the obtained self-supported carbon electrode with NiCo LDH/NiCoS nanoarrays and CC can exhibit superior performance for the electrochemical detection of glucose and  $\text{H}_2\text{O}_2$ .

## 4. Conclusions

In summary, we reported a facile method to construct a self-supported carbon electrode with 2D hybrid NiCo LDH/NiCoS array nanostructures and CC as the substrate, which can be used for glucose and  $\text{H}_2\text{O}_2$  detection. As a glucose and  $\text{H}_2\text{O}_2$

Table 1 Comparison of the important characteristic parameters of the NiCo LDH/NiCoS/CC electrode with other reported non-enzymatic bifunctional electrodes for glucose and  $\text{H}_2\text{O}_2$  detection

Electrode	Glucose			$\text{H}_2\text{O}_2$			Ref.
	Sensitivity ( $\mu\text{A mM}^{-1} \text{cm}^{-2}$ )	Linear range (mM)	LOD ( $\mu\text{M}$ )	Sensitivity ( $\mu\text{A mM}^{-1} \text{cm}^{-2}$ )	Linear range (mM)	LOD ( $\mu\text{M}$ )	
CoS/GCE	28.44	1.2–10.2	1.5	17.4	0.005–14.82	1.5	55
$\text{Ni}_{5.5}\text{Co}_{1.5}\text{S}_6/\text{GCE}$	494.58	0.005–0.5	0.15	94.79	0.005–15.09	0.15	56
$\text{Ni}_7\text{S}_6/\text{GCE}$	271.8	0.005–3.7	0.15	37.77	0.005–20.5	0.15	57
$\text{VS}_2/\text{GCE}$	41.96	0.0005–3	0.211	37.96	0.0005–2.5	0.224	58
Cu–Co alloy/GCE	—	0.0005–14	0.1	—	0.001–11	0.75	59
MCHNs/GCE	52.5	0.001–1.7	0.87	156.6	0.002–0.15	1.03	60
ITO/NiO	1013.76	0.002–0.29	4.6	82.73	0.01–0.87	5.2	61
$\text{Cu}_2\text{S NRs@CF}$	11750.8	0.0002–0.63	0.07	745	0.00025–5	0.12	62
$\text{Co}_3\text{N NW/TM}$	3325.6	0.0001–2.5	0.05	139.9	0.001–12	0.48	32
CuO NRs/FTO	1319	0.005–0.825	—	84.89	0.25–18.75	—	63
$\text{Cu}_2\text{O PLNWs/CF}$	6680.7	0.001–1.8	0.67	1477.3	0.005–1.77	0.13	64
$\text{Fe}_3\text{N-Co}_2\text{N/CC}$	4333.7	0.0001–1	0.077	2273.8	0.00015–8	0.059	65
$\text{CuFe}_2\text{O}_4/\text{NF}$	1239	0.02–5.5	0.22	219.4	0.5–25	0.22	66
Ni/NiO@C	1291	0.01–10	0.116	32.09	0.05–80.7	0.9	31
NiCo LDH/NiCoS/CC	2167, 1417	0.001–3, 4–9	0.208	285	0.01–12	1.66	This work



sensor, it has a wide detection range, outstanding sensitivity, excellent reproducibility and anti-interference ability. The remarkable performance of the obtained self-supported carbon electrode is mainly attributed to the unique 2D ultrathin array nanostructures, abundant interfaces, combination of bimetallic cations and the doping of S element. In addition, the strong synergistic effect between LDH and sulfides further improved the activity and the stability of the self-supported carbon electrode. Our present work demonstrates great promise of a low-cost and self-supported carbon electrode with 2D hybrid nanostructures as a bifunctional electrode for glucose and H<sub>2</sub>O<sub>2</sub> sensors.

## Conflicts of interest

There are no conflicts to declare.

## Acknowledgements

We acknowledge the financial supported by the National Natural Science Foundation of China (No. 51908408, 21872104), the Natural Science Foundation of Tianjin for Distinguished Young Scholar (No. 20JCQJC00150), the Innovative Research Team of Tianjin Municipal Education Commission (TD13-5008) and Tianjin Science and Technology Planning Project (21ZYQCSY00050).

## References

- 1 M. H. Hassan, C. Vyas, B. Grieve and P. Bartolo, *Sensors*, 2021, **21**, 4672.
- 2 G. A. Naikoo, H. Salim, I. U. Hassan, T. Awan, F. Arshad, M. Z. Pedram, W. Ahmed and A. Qurashi, *Front. Chem.*, 2021, **9**, 786.
- 3 M. Adeel, K. Asif, M. M. Rahman, S. Daniele, V. Canzonieri and F. Rizzolio, *Adv. Funct. Mater.*, 2021, **31**, 2106023.
- 4 Y. Hu, M. Hojamberdiev and D. S. Geng, *J. Mater. Chem. C*, 2021, **9**, 6970–6990.
- 5 R. M. Trujillo, D. E. Barraza, M. L. Zamora, A. Cattani-Scholz and R. E. Madrid, *Sensors*, 2021, **21**, 2204.
- 6 Y. Q. Fu and W. Jin, *Mater. Sci. Eng., C*, 2019, **105**, 8.
- 7 X. R. Chen, J. Gao, G. Q. Zhao and C. Wu, *Sens. Actuators, B*, 2020, **313**, 128038.
- 8 D. Q. Yan, L. Zhang, Z. P. Chen, W. P. Xiao and X. F. Yang, *Acta Phys.-Chim. Sin.*, 2021, **37**, 2009054.
- 9 K. N. Zhao, X. Li and D. Su, *Acta Phys.-Chim. Sin.*, 2021, **37**, 2009077.
- 10 Q. Q. Niu, W. B. Lu, C. C. Bao, M. Wei, Z. A. Chen and J. F. Jia, *J. Electroanal. Chem.*, 2020, **874**, 114507.
- 11 D. Z. Chen, D. Pang, S. P. Zhang, H. O. Song, W. Q. Zhu and J. W. Zhu, *Electrochim. Acta*, 2020, **330**, 135326.
- 12 X. Zou, Y. Xu and W. Duan, *The Innovation*, 2021, **2**, 100115.
- 13 J. Zhou, M. Min, Y. Liu, J. Tang and W. Tang, *Sens. Actuators, B*, 2018, **260**, 408–417.
- 14 X. Wang, Y. Zheng, J. Yuan, J. Shen, J. Hu, A.-J. Wang, L. Wu and L. Niu, *Electrochim. Acta*, 2017, **224**, 628–635.
- 15 C. Manjunatha, N. Srinivasa, S. K. Chaitra, M. Sudeep, R. C. Kumar and S. Ashoka, *Mater. Today Energy*, 2020, **16**, 100414.
- 16 S. Liu, K. Wang, M. X. Yang and Z. L. Jin, *Acta Phys.-Chim. Sin.*, 2022, **38**, 2109023.
- 17 C. Gu, H. M. Xu, S. K. Han, M. R. Gao and S. H. Yu, *Chem. Soc. Rev.*, 2021, **50**, 6671–6683.
- 18 Z. H. Huang, C. C. Gu, J. J. Wen, L. L. Zhu, M. Z. Zhang and H. Y. Liu, *NANO*, 2019, **14**, 1950010.
- 19 H. W. Chang, C. W. Su, J. H. Tian and Y. C. Tsai, *Sensors*, 2020, **20**, 4340.
- 20 A. Meng, X. C. Hong, Y. Zhang, S. X. Li, L. Y. Sheng and Z. J. Li, *J. Colloid Interface Sci.*, 2022, **608**, 131–141.
- 21 C. P. Duan, L. L. Wang, J. P. Liu, Y. N. Qu, J. Gao, Y. Y. Yang, B. Wang, J. H. Li, L. L. Zheng, M. Z. Li and Z. Yin, *Chem-ElectroChem*, 2021, **8**, 2272–2281.
- 22 A. Torrinha and S. Morais, *TrAC, Trends Anal. Chem.*, 2021, **142**, 116324.
- 23 J. H. Li, L. L. Wang, H. J. He, Y. Q. Chen, Z. R. Gao, N. Ma, B. Wang, L. L. Zheng, R. L. Li, Y. J. Wei, J. Q. Xu, Y. Xu, B. W. Cheng, Z. Yin and D. Ma, *Nano Res.*, 2022, **15**, 4986–4995.
- 24 Z. Jiang, Z. P. Li, Z. H. Qin, H. Y. Sun, X. L. Jiao and D. R. Chen, *Nanoscale*, 2013, **5**, 11770–11775.
- 25 W. J. Song, X. Teng, Y. Y. Liu, J. Y. Wang, Y. L. Niu, X. M. He, C. Zhang and Z. F. Chen, *Nanoscale*, 2019, **11**, 6401–6409.
- 26 Q. Chen, R. Ding, H. Liu, L. X. Zhou, Y. Wang, Y. Zhang and G. Y. Fan, *ACS Appl. Mater. Interfaces*, 2020, **12**, 12919–12929.
- 27 Z. Yang, Q. H. Cheng, W. W. Li, Y. J. Li, C. Yang, K. Tao and L. Han, *J. Alloys Compd.*, 2021, **850**, 156864.
- 28 G. Yilmaz, K. M. Yam, C. Zhang, H. J. Fan and G. W. Ho, *Adv. Mater.*, 2017, **29**, 1606814.
- 29 Y. X. Chen, C. Jing, X. Fu, M. Shen, K. L. Li, X. Y. Liu, H. C. Yao, Y. X. Zhang and K. X. Yao, *Chem. Eng. J.*, 2020, **384**, 123367.
- 30 D. D. Song, L. L. Wang, Y. N. Qu, B. Wang, Y. T. Li, X. L. Miao, Y. Y. Yang and C. P. Duan, *J. Electrochem. Soc.*, 2019, **166**, B1681–B1688.
- 31 X. Q. Ma, K. L. Tang, M. Y. Yang, W. B. Shi and W. X. Zhao, *J. Mater. Sci.*, 2021, **56**, 442–456.
- 32 F. Y. Xie, X. Q. Cao, F. L. Qu, A. M. Asiri and X. P. Sun, *Sens. Actuators, B*, 2018, **255**, 1254–1261.
- 33 W. Li, S. Lv, Y. Wang, L. Zhang and X. Cui, *Sens. Actuators, B*, 2019, **281**, 652–658.
- 34 X. F. Wei, J. L. Guo, H. T. Lian, X. Y. Sun and B. Liu, *Sens. Actuators, B*, 2021, **329**, 129205.
- 35 D. F. Jiang, Z. Y. Chu, J. M. Peng, J. Y. Luo, Y. Y. Mao, P. Q. Yang and W. Q. Jin, *Electrochim. Acta*, 2018, **270**, 147–155.
- 36 W. W. Li, S. Lv, Y. Wang, L. Zhang and X. Q. Cui, *Sens. Actuators, B*, 2019, **281**, 652–658.
- 37 Y. Li, M. W. Xie, X. P. Zhang, Q. Liu, D. M. Lin, C. G. Xu, F. Y. Xie and X. P. Sun, *Sens. Actuators, B*, 2019, **278**, 126–132.
- 38 S. K. Hassaninejad-Darzi, *J. Electroceram.*, 2014, **33**, 252–263.



- 39 S. K. Hassaninejad-Darzi and M. Gholami-Esfidvajani, *J. Porous Mater.*, 2017, **24**, 85–95.
- 40 J. Y. Chen, Q. Xu, Y. Shu and X. Y. Hu, *Talanta*, 2018, **184**, 136–142.
- 41 S. K. Hassaninejad-Darzi, *RSC Adv.*, 2015, **5**, 105707–105718.
- 42 E. Laviron, *J. Electroanal. Chem. Interfacial Electrochem.*, 1979, **101**, 19–28.
- 43 N. Padmanathan, H. Shao and K. M. Razeeb, *ACS Appl. Mater. Interfaces*, 2018, **10**, 8599–8610.
- 44 X. Q. Cao, K. Y. Wang, G. Du, A. M. Asiri, Y. J. Ma, Q. Lu and X. P. Sun, *J. Mater. Chem. B*, 2016, **4**, 7540–7544.
- 45 J. H. Li, L. L. Wang, Y. Y. Yang, B. Wang, C. P. Duan, L. L. Zheng, R. L. Li, Y. J. Wei, J. Q. Xu and Z. Yin, *Nanotechnology*, 2021, **32**, 505710.
- 46 K. Yuan, Y. C. Zhang, S. H. Huang, S. F. Yang, S. Zhao, F. X. Liu, Q. Y. Peng, Y. P. Zhao, G. Y. Zhang, J. C. Fan and G. C. Zang, *Electroanalysis*, 2021, **33**, 1800–1809.
- 47 Y. H. Dong and J. B. Zheng, *Chem. Eng. J.*, 2020, **392**, 123690.
- 48 J. Gu, Y. Xu, Q. Li and H. Pang, *Chin. Chem. Lett.*, 2021, **32**, 2017–2020.
- 49 Q. Li, Z. Shao, T. Han, M. Zheng and H. Pang, *ACS Sustainable Chem. Eng.*, 2019, **7**, 8986–8992.
- 50 L. L. Wang, Y. Y. Yang, B. Wang, C. P. Duan, J. H. Li, L. L. Zheng, J. H. Li and Z. Yin, *J. Alloys Compd.*, 2021, **885**, 160899.
- 51 L. L. Wang, X. L. Miao, Y. N. Qu, C. P. Duan, B. Wang, Q. L. Yu, J. Gao, D. D. Song, Y. T. Li and Z. Yin, *J. Electroanal. Chem.*, 2020, **858**, 113810.
- 52 Y. Y. Li, L. Tang, D. M. Deng, J. H. Ye, Z. Y. Wu, J. H. Wang and L. Q. Luo, *Colloids Surf., B*, 2019, **179**, 293–298.
- 53 K. Cheng, F. Yang, G. L. Wang, J. L. Yin and D. X. Cao, *J. Mater. Chem. A*, 2013, **1**, 1669–1676.
- 54 Z. Y. Yang, S. Zhang, Y. Y. Fu, X. H. Zheng and J. B. Zheng, *Electrochim. Acta*, 2017, **255**, 23–30.
- 55 W. Q. Wu, B. B. Yu, H. M. Wu, S. F. Wang, Q. H. Xia and Y. Ding, *Mater. Sci. Eng., C*, 2017, **70**, 430–437.
- 56 W. Q. Wu, L. W. Wu, H. M. Wu, S. F. Wang, Y. Ding and C. Q. Feng, *Sens. Actuators, B*, 2017, **250**, 224–232.
- 57 W. Q. Wu, Y. B. Li, J. Y. Jin, H. M. Wu, S. F. Wang and Q. H. Xia, *Sens. Actuators, B*, 2016, **232**, 633–641.
- 58 A. Sarkar, A. B. Ghosh, N. Saha, G. R. Bhadu and B. Adhikary, *ACS Appl. Nano Mater.*, 2018, **1**, 1339–1347.
- 59 H. B. Noh, K. S. Lee, P. Chandra, M. S. Won and Y. B. Shim, *Electrochim. Acta*, 2012, **61**, 36–43.
- 60 Z. Y. Gao, J. L. Liu, J. L. Chang, D. P. Wu, J. J. He, K. Wang, F. Xu and K. Jiang, *CrystEngComm*, 2012, **14**, 6639–6646.
- 61 S. Jana, G. Mondal, B. C. Mitra, P. Bera, B. Chakraborty, A. Mondal and A. Ghosh, *New J. Chem.*, 2017, **41**, 14985–14994.
- 62 W. D. Lu, Y. J. Sun, H. C. Dai, P. J. Ni, S. Jiang, Y. L. Wang, Z. Li and Z. Li, *RSC Adv.*, 2016, **6**, 90732–90738.
- 63 P. Chakraborty, S. Dhara, K. Debnath and S. P. Mondal, *J. Electroanal. Chem.*, 2019, **833**, 213–220.
- 64 W. D. Lu, Y. J. Sun, H. C. Dai, P. J. Ni, S. Jiang, Y. L. Wang, Z. Li and Z. Li, *Sens. Actuators, B*, 2016, **231**, 860–866.
- 65 D. Zhou, X. Q. Cao, Z. Wang, S. Hao, X. D. Hou, F. L. Qu, G. Du, A. M. Asiri, C. B. Zheng and X. P. Sun, *Chem. – Eur. J.*, 2017, **23**, 5214–5218.
- 66 H. Y. Xia, J. A. Li, L. Ma, Q. F. Liu and J. B. Wang, *J. Alloys Compd.*, 2018, **739**, 764–770.
- 67 W. Li, X. Guo, P. Geng, M. Du, Q. Jing, X. Chen, G. Zhang, H. Li, Q. Xu, P. Braunstein and H. Pang, *Adv. Mater.*, 2021, **33**, 2105163.
- 68 P. Geng, L. Wang, M. Du, Y. Bai, W. Li, Y. Liu, S. Chen, P. Braunstein, Q. Xu and H. Pang, *Adv. Mater.*, 2022, **34**, 2107836.
- 69 X. Li and Q.-L. Zhu, *EnergyChem*, 2020, **2**, 100033.

